

SUPPLEMENTARY INFORMATION

Optical Clearing Delivers Ultrasensitive Hyperspectral Dark-Field Imaging for Single-Cell Evaluation

*Yi Cui[‡], Xiaolei Wang[‡], Wen Ren, Jing Liu[†], and Joseph Irudayaraj**

Department of Agricultural and Biological Engineering, Bindley Bioscience Center, Birck Nanotechnology Center, Purdue Center for Cancer Research, Purdue University, West Lafayette, IN 47907, United States

[‡]These authors contributed equally to this work

[†]Current address: Department of Nanoscience and Nanoengineering, South Dakota School of Mines & Technology, Rapid City, SD 57701

*Corresponding author. E-mail: josephi@purdue.edu; Tel: +1 (765)494-0388

Supplementary Methods and Materials

1. *HSDFM instrumentation and image processing.* A home-built hyperspectral dark-field imaging system was used to conduct experiments and demonstrate the significance of optical clearing. The whole instrumentation, based on an Olympus BX51 microscope, was installed on a vibration-reducing optical breadboard (Thorlabs). A tungsten halogen light source (3900, Illumination Technologies) with highly stable output (fluctuation < 0.1%) was coupled to a CytoViva condenser (N.A 1.2-1.4) via a fiber optic light guide, which minimized the thermal fluctuation from the light source. Pre-aligned Koehler illumination precisely focused the tungsten halogen source onto the entrance slit of the condenser. Combining pre-aligned Koehler, critical illumination with structured illumination in the dark-field condenser enables an exquisite spatial resolution. A motorized stepper Prior stage with a minimum step size of 40 nm (H101A, Prior Scientific) was equipped for collecting hyperspectral data during scanning. This finer step size significantly increased the spatial resolution for reconstruction of spectral maps. The scattering light was collected with a 100× oil objective with an iris, and then split into two light paths: one for real-time dark-field imaging, the other for hyperspectral measurement. The scattered light shed on a narrow slit of the spectrograph and generated a one dimensional (1D) profile. The 1D profile was dispersed by a grating in the spectrograph and then collected by a CCD camera (PIXIS-400BR, Princeton Instruments). The spectrograph (SP2150, Princeton Instruments) includes dual-indexable gratings (300 g/mm and 1200 g/mm) and a direct digital grating/scanning module with capabilities for dual-grating imaging and full-wavelength scanning. The astigmatism-corrected optical module, the adjustable slit width with a smallest gap size of 10 nm, the fine grating in the spectrograph, and the very low dark noise of the CCD together contributed to the outstanding resolution and SNR of hyperspectral images.

In order to obtain hyperspectral images of the nanoprobe with high SNR, intensity and wavelength filters were needed for the removal of parasitic noise, as well as noises from dusts, glassware defects, and non-specific aggregates of nanoprobe. Acquiring images at a specific wavelength comprises three main steps: (i) wavelength screening; (ii) signal normalization; (iii) determination of spectral filter and intensity threshold. 1D spectra images from homogeneous nanoprobe were used to obtain an approximate wavelength window at the full width at half maximum (FWHM). Since the illumination from the incident source per se was not constant over the whole range of wavelengths, the obtained signals by detector should be normalized to a proper background to extract the true scattering spectra. For *in vitro* and *in vivo* nanoprobe,

the reference background was different: the *in vitro* nanoprobe signal was normalized to the spectrum of halogen source, while the *in vivo* nanoprobe signal was normalized to the spectrum of the cellular background. Notably, the scattering profile from optically cleared cells was obtained to normalize the signal of intracellular nanoprobe. Ten representative scattering spectra from reference cellular compartments were averaged to facilitate signal normalization and intensity filtering. Scattering from the defects of optical glassware, dusts, and non-specific nanoprobe aggregates can also be filtered out by setting appropriate intensity thresholds and spectral filters. Since the signals of nanoprobe are significantly stronger than the background noise after clearing treatments, single nanoprobe can be easily identified. Only signals from pre-determined ROI were included for processing. For image reconstruction, with the preset wavelength range and intensity threshold, the collected 1D spectral data were stacked and a 2D image at the desired wavelength channel was generated. From this image, the spatial distribution and quantity of nanoprobe (the biomolecule targets by extension) can be determined. Based on the hyperspectral data set, the peak wavelength of scattering at each pixel can be extracted to reconstruct a spectral map. According to the spectral map, the regional density of the target can be inferred.

For processing the images in multiplexing detection, the co-existence of GNP and GNR in a single pixel can be distinguished by analyzing the intensity ratio of 687 nm to 547 nm. As the GNP and GNR peaks are present, the number of them can be obtained by:

$$N_{GNR} = I_{687} / \varepsilon_{GNR-L}$$

$$N_{GNP} = (I_{547} - N_{GNR} \cdot \varepsilon_{GNR-T}) / \varepsilon_{GNP}$$

where I is the detected intensity at a specific wavelength, ε_{GNP} is the unit intensity for a single GNP, ε_{GNR-L} and ε_{GNR-T} are the unit intensities for the GNR longitudinal and transverse modes, respectively. However, considering the size of plasmonic probes and the optical diffraction limit, the chance to get multiple GNPs and GNRs in a single pixel is quite low, which was less observed when we reconstructed a spectral map. Given such a pixel, its spectral peak was calculated as a probe number-weighted average value using the GNP peak and the GNR longitudinal peak.

2. *Optical clearing for zebrafish embryo and human breast tissue slice.* 6 hpf zebrafish embryos were fixed with 4% paraformaldehyde at 4°C overnight, and dechorionated the next day. Before optical clearing, the embryo yolk was also removed. The cleared embryos were

incubated with GNPs and placed onto clean glass slides coated by poly-L-lysine for imaging (**Supplementary Fig. 5**). For paraffin embedded human breast tissue slices (~5 μm in thickness), the samples were deparaffinized with serial immersion into 100% xylene (6 min), xylene 1:1 with ethanol (3 min), 100% ethanol (6 min), 95% ethanol (3 min), 70% ethanol (3 min), 50% ethanol (3 min) solutions before optical clearing. Representative images of cleared tissue are shown in the **Supplementary Fig. 6**.

3. *Algorithm for centroid extraction*. The centroid location of nanoprobe was extracted based on the Laplacian of Gaussian (LOG) function. The Laplacian function is a 2D isotropic measure of the second spatial derivative, which can detect the region with abrupt intensity changes and is therefore often used for edge finding. Since the second derivative function is sensitive to background noise, a Laplacian function is applied after smoothing the image with a Gaussian function. The combination of these two functions is integrated into an imageJ plugin. The Laplacian function $L(x,y)$ is defined as

$$L(x,y) = \frac{\partial^2 I(x,y)}{\partial x^2} + \frac{\partial^2 I(x,y)}{\partial y^2}$$

where $I(x,y)$ is the intensity at each pixel. This equation can be calculated using a convolution kernel that approximates the Laplacian function based on the image matrix. The convolution operation is associative: the Gaussian smoothing function is first convolved with the Laplacian function, and then this hybrid filter rolls over the image at the base of single kernels. The 2D LOG filter with the Gaussian standard deviation σ is expressed as

$$LOG(x,y) = -\frac{1}{\pi\sigma^4} \left(1 - \frac{x^2 + y^2}{2\sigma^2} \right) e^{-\frac{x^2 + y^2}{2\sigma^2}}$$

This filter function for locating the centroid of nanoprobe is subjected to the kernel size and predetermined intensity threshold, and hence calibration of these parameters is needed before each set of experiments (**Supplementary Fig. 8**).

4. *SRS imaging microscopy*: The label-free imaging for lipids in cells was performed with a home-built femtosecond pump-probe microscopy which featured a SRS imaging modality. **Supplementary Fig. 10** shows the microscope layout. Briefly, a Ti:Sapphire laser (Chameleon Ultra, Coherent) provided an output pulse train at 800 nm with the pulse duration of 170 fs and repetition frequency of 80 MHz, which served as the pump beam. A portion of the pump beam

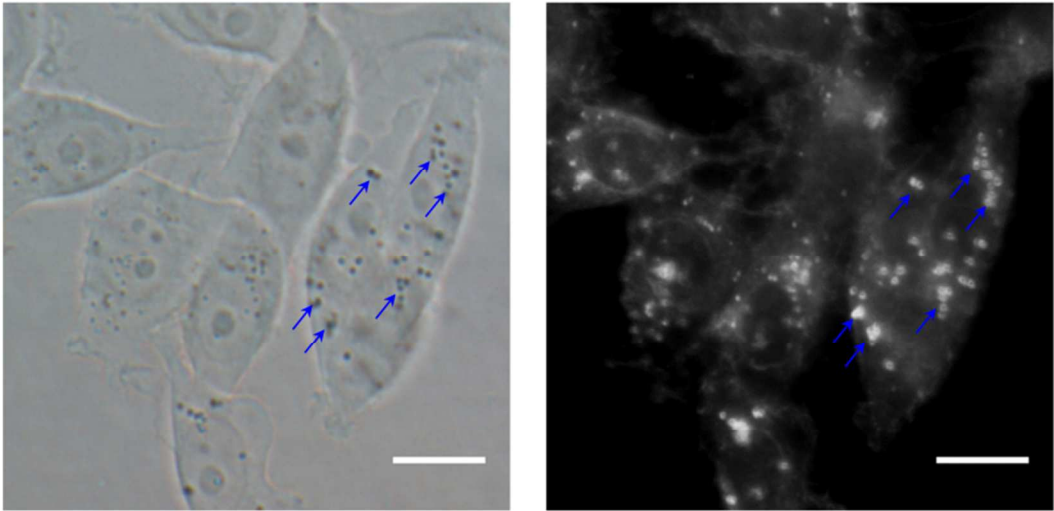
was directed to an optical parameter oscillator (OPO, Coherent Inc.) to produce the synchronized pulse train from 1000 nm to 1500 nm, which served as the probe beam (the idler beam was blocked). The intensity of the probe beam was sinusoidally modulated by an acoustic-optical modulator (AOM, 3080-122, Crystal Technology) at 2.4 MHz. Both the pump and probe beams were then spatially overlapped by a dichroic mirror (z1064rdc-sp, Chroma) and temporally overlapped by a home-made delay stage. The SRS signal was then calibrated with pure DMSO. For cell imaging, the collimated pump and probe beams were delivered to a laser scanning unit (C1, Nikon) which was customized to fit with an inverted near-infrared multi-photon microscope (IX71, Olympus). The scanning mirror in the C1 unit was projected to the back pupil of a water immersion objective lens (UPlanApo/IR, Olympus; NA 1.2, 60 \times); transmitted beams through the sample were collected with an oil immersion objective lens (UPlanSApo, Olympus; NA 1.3, 60 \times). A telescope was then used to project the signal onto a large-area photodiode (FDS1010, Thorlabs) to mitigate the beam shift when scanning. The photodiode was reversely biased of 48 V. Three high OD band-pass filters (ET810/90m, Chroma) were used to block the probe beam. The output current of the photodiode was terminated with 50 Ω resist and then connected to a high-frequency lock-in amplifier (SRS844RF, Stanford Research Systems) to demodulate the stimulated Raman loss signal of the pump beam. The in-phase component output of the lock-in amplifier was fed into the input of control unit of the scanners. The pump-probe microscopy worked in a beam-scanning mode. All SRS images were acquired at 512 \times 512 pixels with the dwelling time of 38.16 μ s for each pixel; laser powers after the excitation objective used in the experiment were: 5 mW for pump beam, 20 mW for modulated probe beam in 2845 cm^{-1} and 2950 cm^{-1} .

Supplementary Table

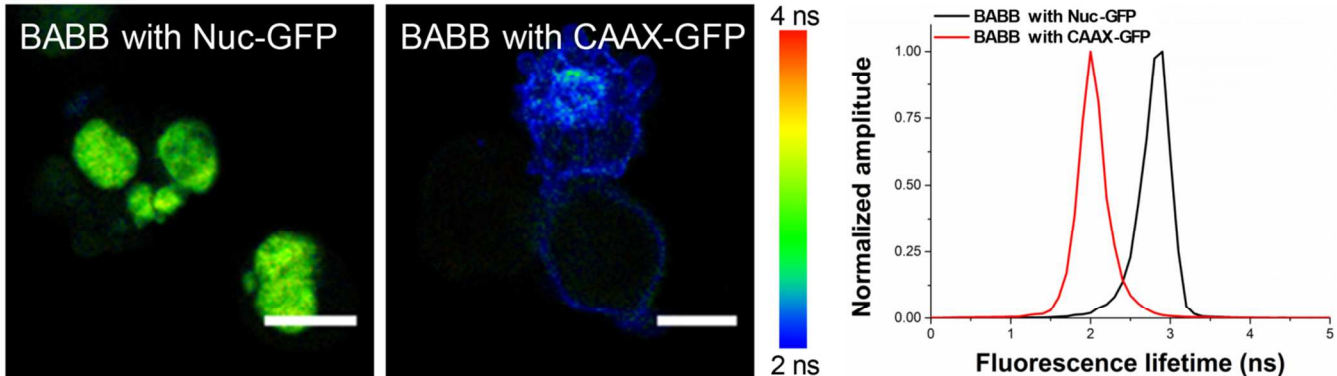
	Fluorescence microscopy	Hyperspectral dark-field microscopy
Illumination source	various wavelengths for different fluorochromes	normal white illumination
Photo-bleaching	yes	no
Photo-damage	possibly high	low
SNR	depends on the quantum efficiency of fluorochrome	high when using plasmonic nanomaterials (10-10,000 folds stronger than fluorescence in cross section)
Background noise	subjected to auto-fluorescence, scattering, and non-specific signals	can be greatly attenuated by filtering the spectral fingerprint of a nanoprobe
Imaging speed	fast for wide-field microscopy	relatively slower than wide-field systems; faster than point-scanning confocal system
Multiplexing capability	yes; but subjected to signal bleed-through	yes; but need highly uniform nanoprobe
Measurement of Inter-molecule interaction	< 10 nm for FRET	tunable based on the size of particles (e.g., ~20 nm when using 40 nm GNPs)

Supplementary Table 1 Comparison between fluorescence microscopy and hyperspectral dark-field microscopy.

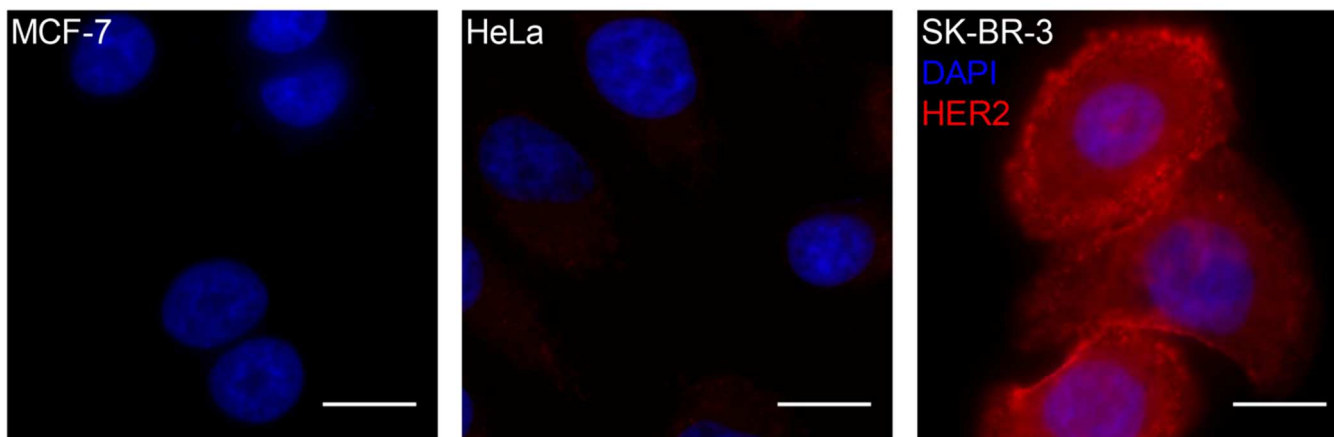
Supplementary Figures



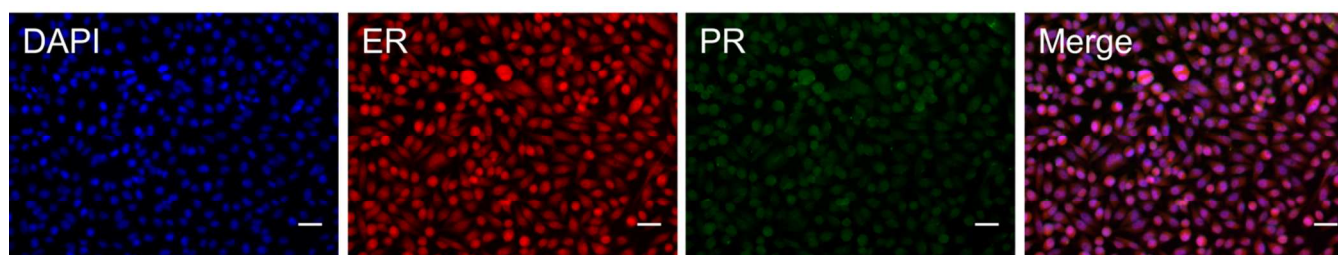
Supplementary Figure 1 Contrast comparison between the bright-field and dark-field imaging for intracellular strong scatterers. (Scale bars: 10 μ m)



Supplementary Figure 2 FLIM images of HeLa cells with nuclear GFP or membrane GFP after optical clearing using BABB. (Scale bars: 10 μ m)

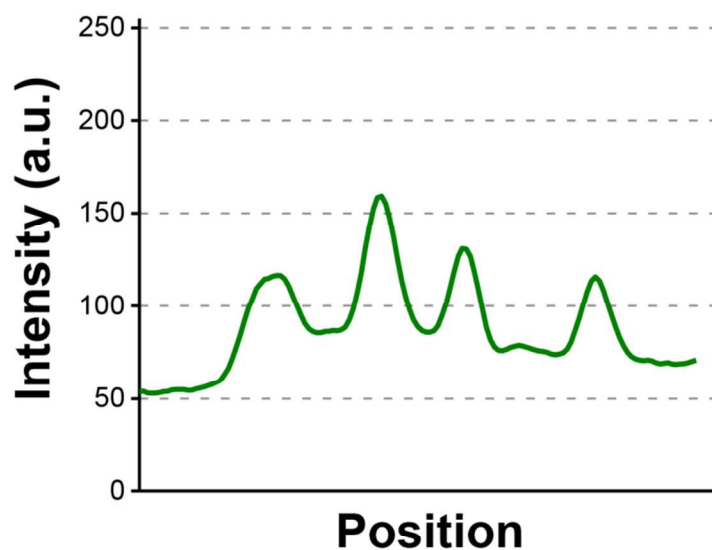
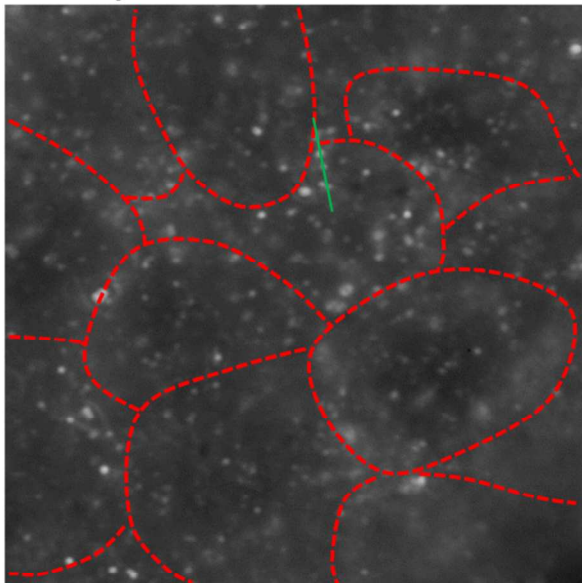


Supplementary Figure 3 Fluorescence images of the HER2 protein in three different cancer cell lines. HER2 was labeled with anti-rabbit-IgG-Alexa546. (Scale bars: 10 μ m)

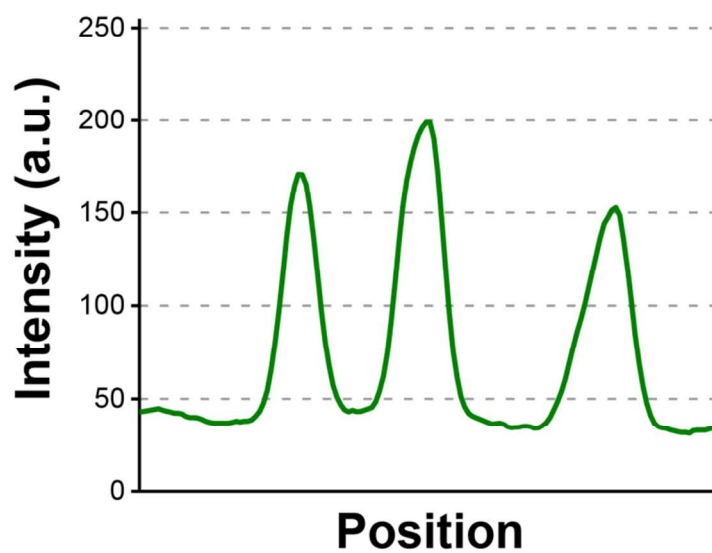
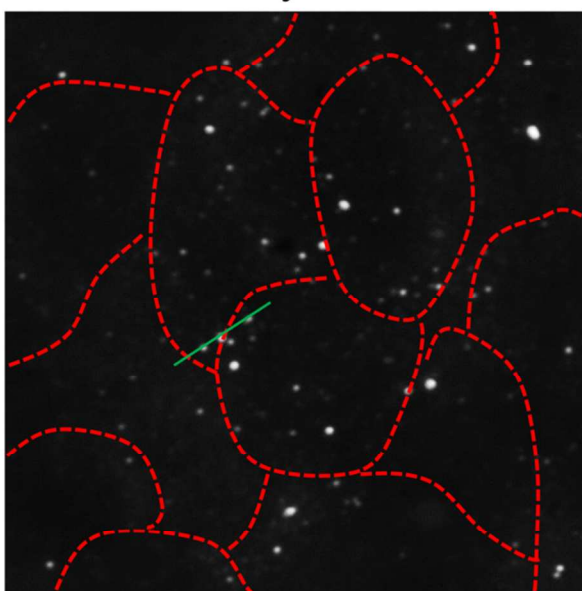


Supplementary Figure 4 Fluorescence images of the modified ER-expressing HeLa cells where the PR expression can be moderately activated by the ER pathway. Primary antibodies of different host species were obtained from Santa Cruz Biotechnology, Inc. ER and PR were labeled with Alexa546 and Alexa488, respectively.

Embryo + GNPs

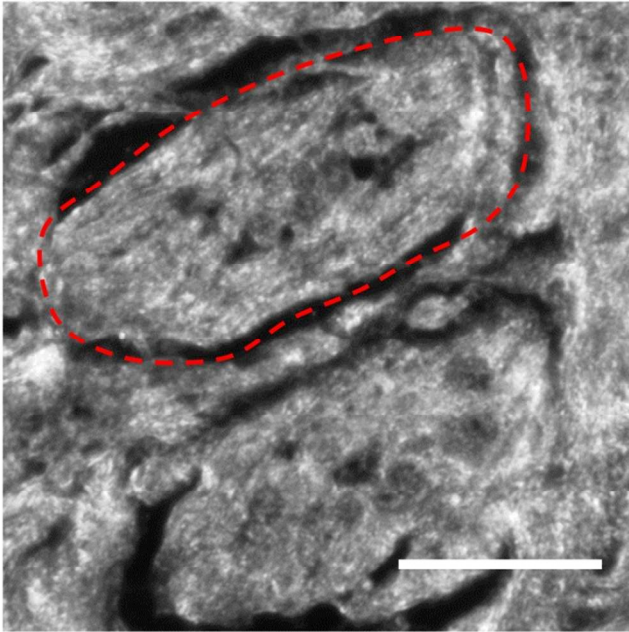


Cleared embryo + GNPs

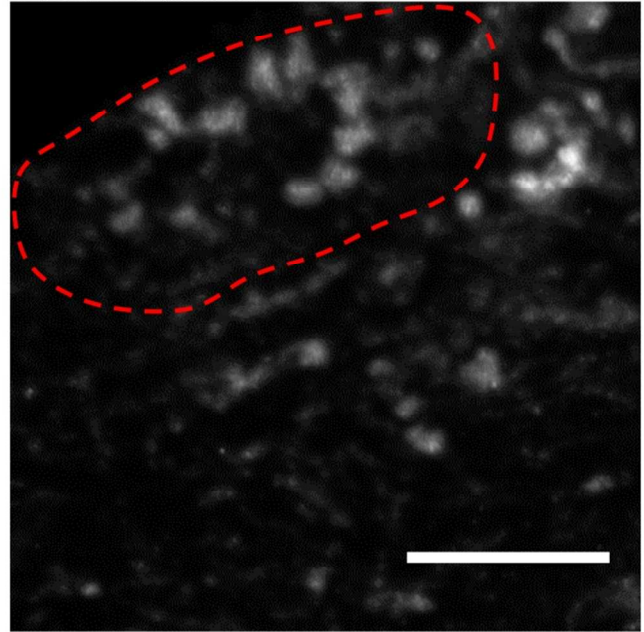


Supplementary Figure 5 Dark-field images of zebrafish embryos incubated with GNPs before and after optical clearing. The intensity profiles cross an indicated line (green) are provided to show the improvement of SNR.

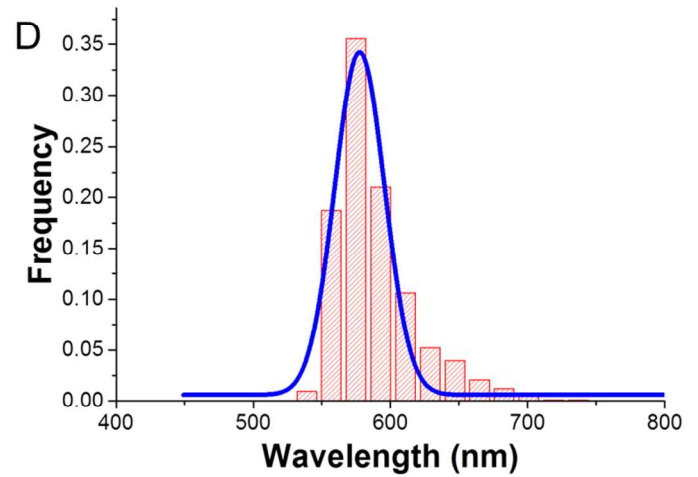
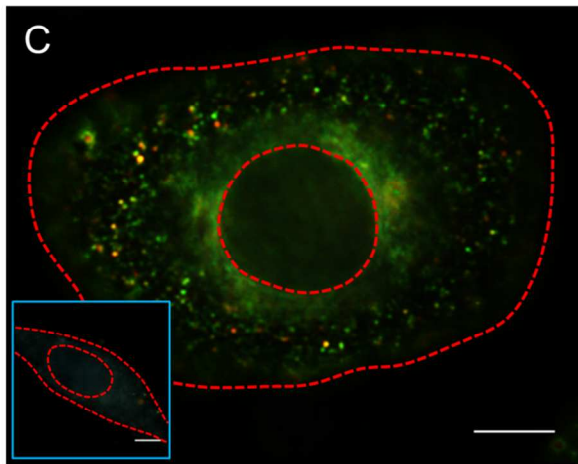
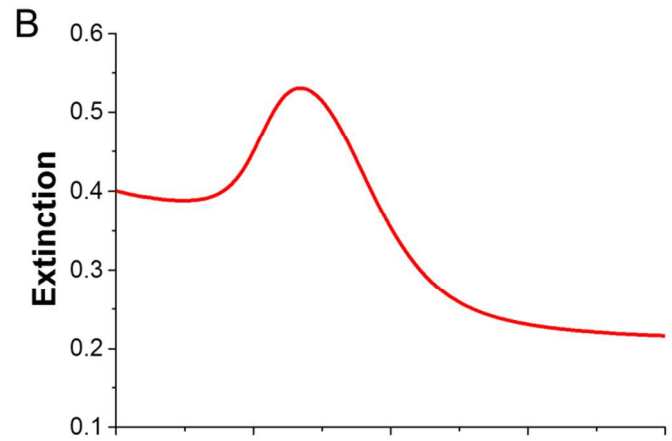
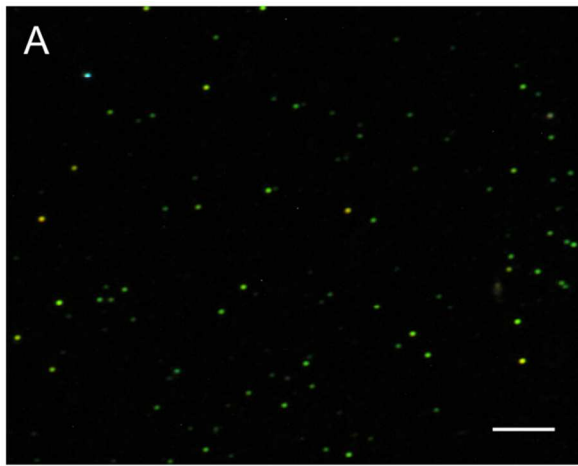
Raw tissue



Cleared tissue

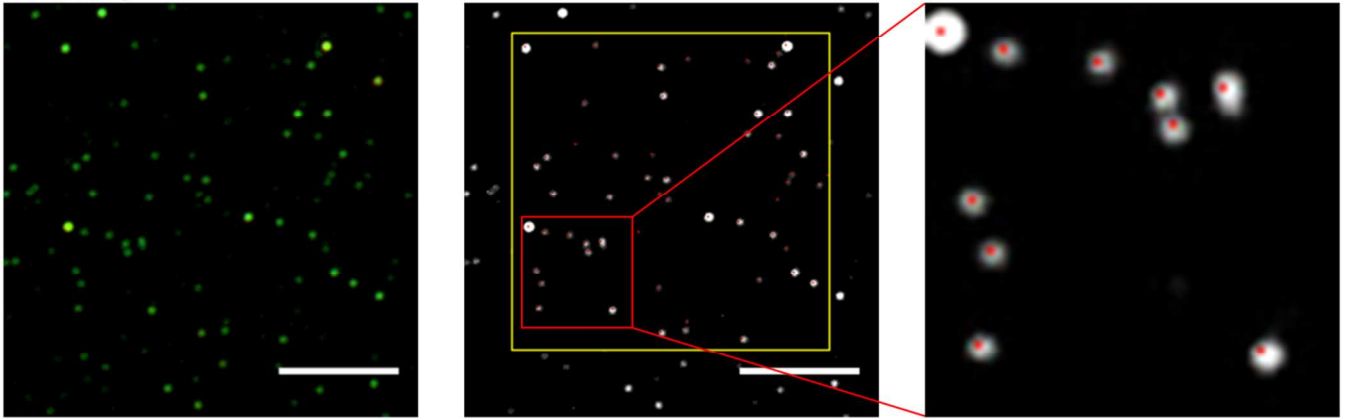


Supplementary Figure 6 Scattering from a human breast tissue slice before and after optical clearing. The circled regions are a typical mammary gland. (*Exposure time: 0.8 s; Scale bars: 20 μm*)

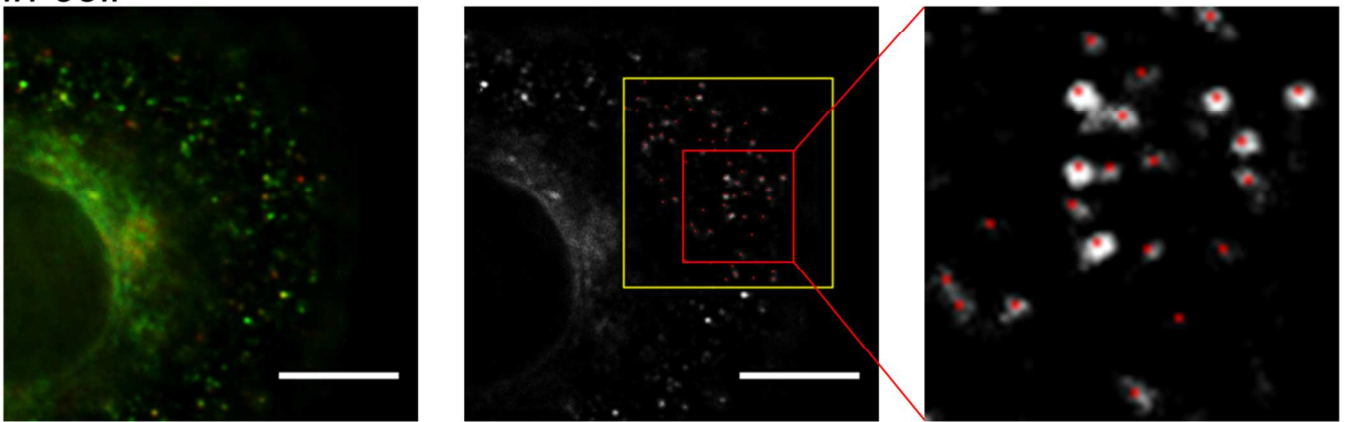


Supplementary Figure 7 Characterization for the conjugated DNA-GNP nanoprobe. (A) A dark-field image of the probes dispersed in phosphate buffer. (B) UV-vis spectrum of the probe solution. (C) HER2 probes in a SK-BR-3 cell. Cell incubated with scrambled probes is also presented (inset). (Scale bars: 10 μm) (D) Histogram of scattering peak wavelengths extracted from the intracellular nanoprobe.

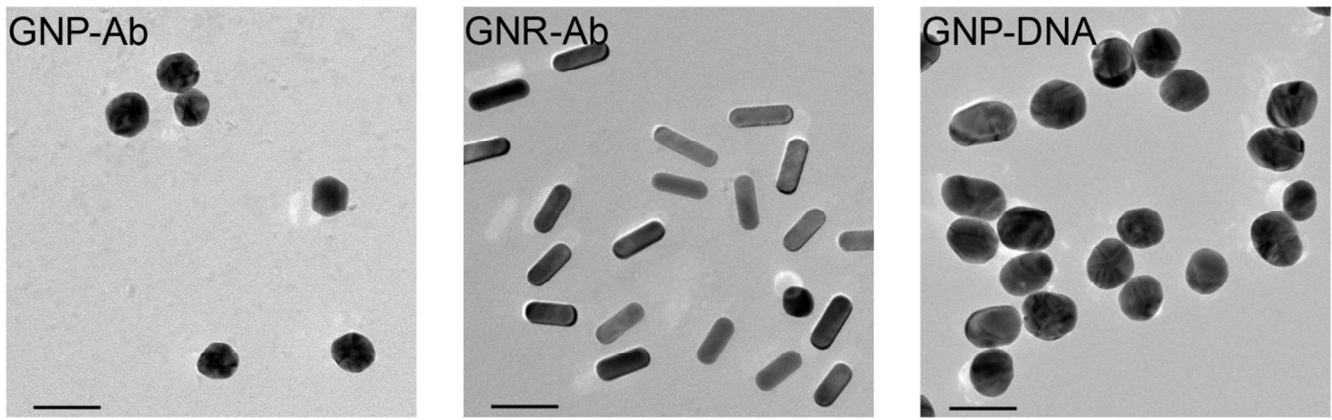
in vitro



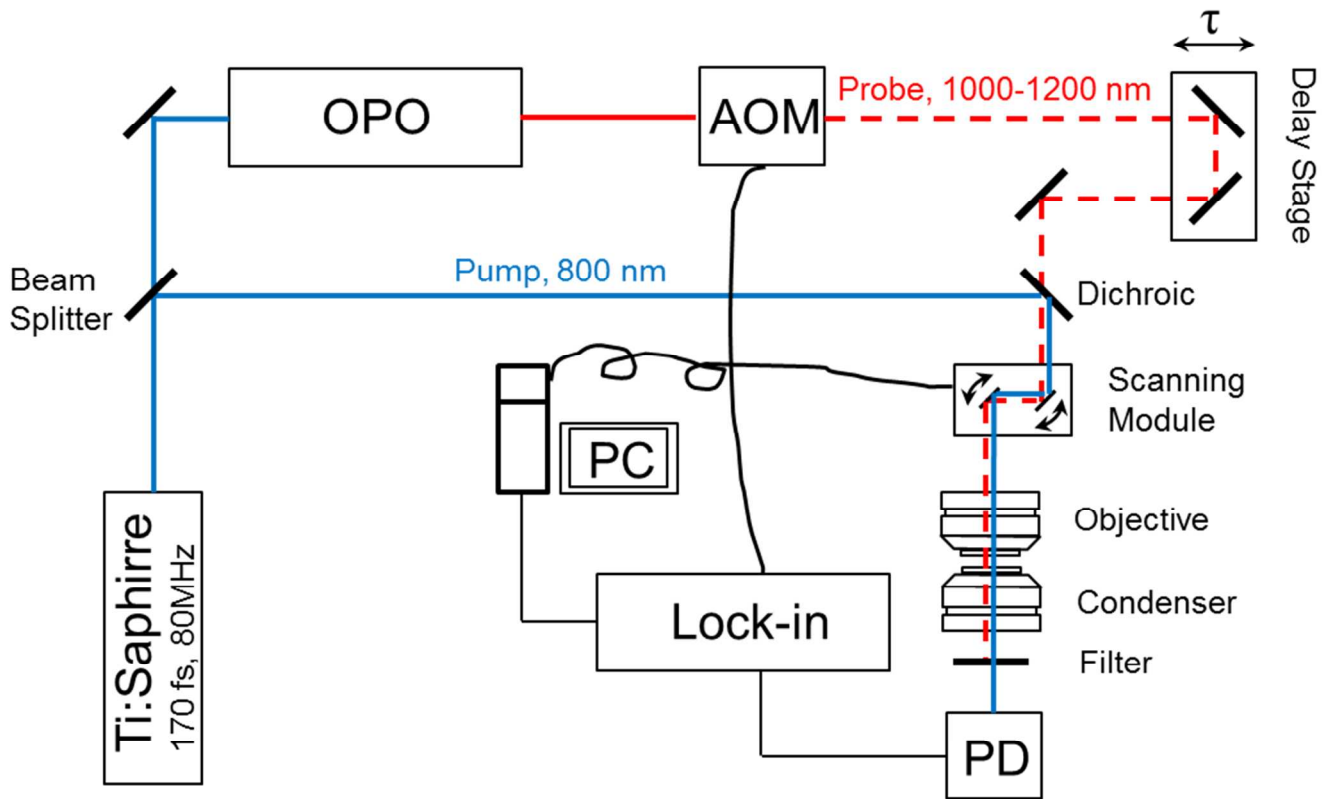
in cell



Supplementary Figure 8 LOG function for locating the centroid of nanoprobes.



Supplementary Figure 9 Representative TEM images of all nanoprobes used in this study. (Scale bars: 50 nm)



Supplementary Figure 10 Optical layout of the SRS microscope.